# Structure and Formation of the Lunar Farside Highlands

Ian Garrick-Bethell,[1]*† Francis Nimmo,[2] Mark A. Wieczorek[3]

The formation of the lunar farside highlands has long been an open problem in lunar science. We show that much of the topography and crustal thickness in this terrain can be described by a degree-2 harmonic. No other portion of the Moon exhibits comparable degree-2 structure. The quantified structure of the farside highlands unites them with the nearside and suggests a relation between lunar crustal structure, nearside volcanism, and heat-producing elements. The farside topography cannot be explained by a frozen-in tidal bulge. However, the farside crustal thickness and the topography it produces may have been caused by spatial variations in tidal heating when the ancient crust was decoupled from the mantle by a liquid magma ocean, similar to Europa's present ice shell.

Since the Apollo 15 laser altimeter experiment, it has been widely known that the topography of the lunar farside highlands is the highest on the Moon (*1*). This elevated region makes up a large part of the Feldspathic Highlands Terrane (FHT), the largest of the Moon's three major geologic provinces (*2*). Because the farside highlands may be a relict of very early thermal processes (*2*, *3*), understanding their structure and formation may help constrain models of global lunar evolution and magma-ocean processes in general (*4*). Theories for the formation of the farside highlands include South Pole–Aitken (SP-A) basin ejecta deposits (*5*), asymmetric nearside/farside cratering (*6*), magma-ocean convective asymmetries (*7*), and asymmetric crustal growth (*3*). However, there has been no quantitative description of the farside highlands to date; therefore, models that describe their formation are poorly constrained.

Here, we analyze global topography (*8*) and gravity data sets (*9*) to better describe the lunar farside highlands. We fit the mean topography from five swaths of terrain centered in the farside highlands to a degree-2 Legendre polynomial $P_2$ [Fig. 1, supporting online material (SOM), fig. S2] in north, northeast, and east directions (Fig. 1A, black portion of topography profile, 0° to between 95° and 105° of arc). We used a variety of swath centers because of the uncertainty in the exact terrain center. The fit to $P_2$ is excellent in all cases (correlation coefficient $R^2 > 0.93$), and two additional observations allow us to confirm that the terrain is indeed described by $P_2$. First, for swaths 1 to 3, the fits accurately predict the topography encountered in the western, southwestern, and southeastern portions of the swaths for at least 55° of arc (~1700 km, leftmost blue section of topography profiles; figs. S2 and S8). Second, the entire northern-, northeastern-, and eastern-directed decrease in topography on the lunar farside takes place over ~90° of arc, as expected from a $P_2$ function. A global search revealed that no other region of the Moon exhibits comparable degree-2 structure (figs. S4 to S7), including all of the nearside, despite the Moon's well-known high degree-2 topography and gravity spherical harmonic coefficients.

We have also applied the same swath fitting analysis described above to a crustal-thickness model derived from topography (*8*) and gravity data (*9*) (SOM). We find that all of the same trends in topography are also observed in crustal thickness (Fig. 1, C and D), indicating that the farside highlands topography is largely due to crustal-thickness variations, as inferred previously (*1*). Using the average values of the fitted regions in swaths 1 to 5, the maximum crustal thickness is 76 km, and the minimum is 40 km (amplitude of ~36 km).

The maximum amplitude and center of the terrain described by a $P_2$ function is near 0° ± 5°N, 215° ± 5°E, close to the direction of the center-of-mass/center-of-figure offset at 8°N, 203°E (*10*). Overall, the region fit by $P_2$ comprises ~24% of the lunar surface, and, for convenience, we refer to it here as the DTT (degree-2 terrain).

Two observations suggest that ejecta from the neighboring SP-A basin had a minimal effect on the DTT and farside highlands and that SP-A postdates their formation. First, the DTT topography obeys a $P_2$ function that is centered external to and northeast of the basin, and there are no models for ejecta production that would explain such an unusual distribution. The lack of an extensive ejecta deposit for SP-A is consistent with anomalously low excavated volumes for this and the next two largest lunar basins (*11*). Second, a comparison of swaths 4 and 5, which extend into SP-A's depression, with swaths 1 to 3, suggests that SP-A is superimposed on a longer wavelength $P_2$ shape in the south and southwest. Therefore, because of the great antiquity of SP-A, the $P_2$ shape of the DTT is probably the Moon's most primordial feature, in agreement with (*12*).

The DTT extends for ~40° of arc into the lunar nearside, crossing mare units in Oceanus Procellarum and parts of Mare Frigoris (Fig. 1), thereby linking two traditionally separate geologic units: the farside FHT and the Procellarum KREEP Terrane (PKT) (*2*). Profiles of crustal thickness and topography along the borders of both units are relatively constant (SOM, fig. S17). This continuity and constancy of border data suggest a related early geologic history for both provinces and that the borders of Oceanus Procellarum and Mare Frigoris are related to long-wavelength crustal structure (Fig. 1D). The DTT structure is also undisturbed across the rim of the putative Procellarum impact basin that has been suggested to produce a number of nearside-farside differences (*13*). Therefore, either the Procellarum basin formed well before complete crust formation, or it never formed. Finally, if the DTT center was once nearer to 0°N, 180°E, as implied by the tidal-heating calculations developed below, it would imply the Moon's minimum moment of inertia axis has shifted only ~35° since crust formation.

The DTT must have formed very early in lunar thermal evolution, because its crust is nearly compensated, as indicated by the regional lack of strong positive free-air gravity anomalies (*9*) (SOM). In order for such compensation to have taken place, the Moon must have still been very hot, probably <100 million years (My) after accretion (*14*), when a subsurface magma ocean was likely present (*15*, *16*).

The DTT follows a $P_2$ function like that expected from a tidal process, but it cannot have been formed entirely by freezing in an ancient tidal bulge (*17*), because such a bulge would not cause crustal-thickness variations. In addition, a hydrostatic tide of 6.4-km amplitude (mean of swaths 1 to 5) exists at a semimajor axis of ~12 Earth radii ($R_E$). The Moon evolved to this location only ~$10^6$ years after accretion (SOM) and was certainly too hot and its lithosphere too thin to retain such a bulge.

Predominantly degree-2 crustal-thickness variations similar to those in the DTT may arise in tidally heated satellites with subsurface liquid oceans, such as Europa (*18*–*20*) and Titan (*21*). The subsurface ocean decouples the crust from the mantle and leads to high tidal dissipation in the crust's warm base. This dissipation serves as a heat source within the crust, such that the crust will be thinner relative to its thickness without dissipation (*18*). Because dissipation is greatest at the poles and least at the equatorial 0° and 180° longitudes, the crust becomes thinner and thicker in those locations, respectively, for low-obliquity orbits. Like Europa, the Moon also once possessed an ocean beneath its crust.

We calculated the tidal heating in a floating anorthositic lunar crust (*19*) with a temperature-dependent viscosity (*22*) (SOM). We assumed

[1]Department of Geological Sciences, Brown University, Providence, RI 02912, USA. [2]Department of Earth and Planetary Sciences, University of California, Santa Cruz, 1156 High Street, Santa Cruz, CA 95064, USA. [3]Institut de Physique du Globe de Paris - Sorbonne Paris Cité, Paris, France.

*To whom correspondence should be addressed. E-mail: igarrick@ucsc.edu

†Present address: Department of Earth and Planetary Sciences, University of California, Santa Cruz, 1156 High Street, Santa Cruz, CA 95064, USA.

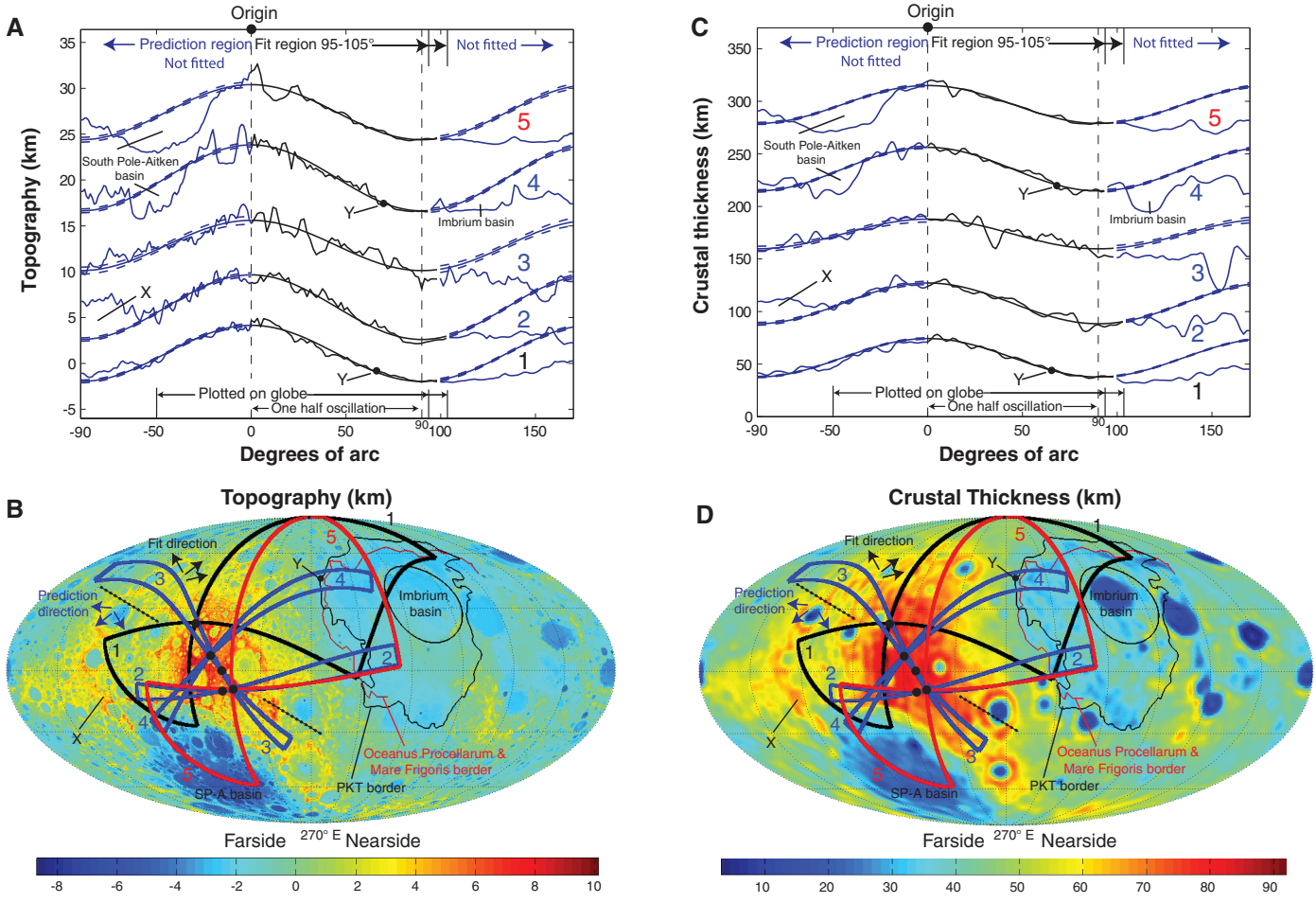


**Fig. 1.** The degree-2 structure of the lunar farside highlands. (**A**) Mean topography inside the five great-circle swaths shown in (B), fitted to a $P_2$ function in the black region, and vertically offset for clarity. Data and fitted $P_2$ function beyond the fit region are illustrated in blue with 95% confidence intervals (dashed lines). Vertical axis applies to swath 1 only, but scale is constant throughout. X, region described by a possible degree-4 harmonic (see text and Fig. 2A); Y, point on the PKT border and central to swaths 1 and 4. (**B**) Portions of swaths from (A) plotted over topography data (*8*). Swaths 1 (black) and 5 (red) are averages over large regions. The PKT boundary is based on the 3.5–parts per million thorium contour (*2*). Points X and Y from (A) are shown. Black and blue arrows indicate fit and prediction directions, respectively. (**C**) and (**D**) Same as (A) and (B), but for crustal thickness.

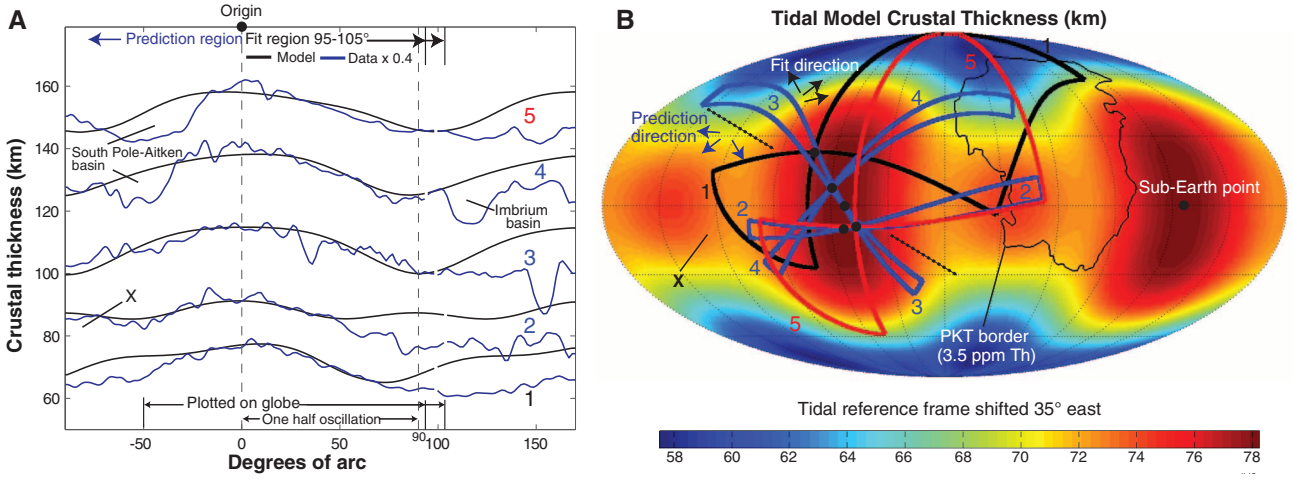


**Fig. 2.** Lunar crustal thickness compared with a tidal-dissipation model. (**A**) Mean profiles of lunar crustal-thickness swaths derived from tidal dissipation at $a = 20\ R_E$, $e = 0.02$, $T_b = 1175$°C, and $q_o = 27$ mW/m$^2$ (black lines), along with the profiles from Fig. 1C (multiplied by 0.4, blue lines, arbitrarily offset). Swath dimensions are the same as in Fig. 1. Vertical axis applies to model swath 1 only, but scale is constant throughout. Fit directions are indicated, but no fits were performed in this figure. (**B**) Map of crustal thickness used for (A). Model data in both (A) and (B) have been shifted 35° east, because the DTT center is ~35° east of the theoretical maximum crustal thickness at 0°N, 180°E. Compare with Fig. 1, C and D; see also fig. S10.

synchronous rotation and that the crust is in conductive thermal equilibrium with tidal heating and an additional basal heat flux ($q_o$) from mantle cooling and radiogenic heat. Important parameters are the eccentricity ($e$), semimajor axis ($a$), and magma-ocean temperature ($T_b$). We calculate that, 100 My after accretion, there was an approximate mean basal heat flux of ~27 mW/m$^2$: ~20 mW/m$^2$ from radiogenic magma-ocean liquids and ~7 mW/m$^2$ from mantle cooling (SOM).

We find that crustal-thickness differences of 21 km (mean = 65 km, minimum = 50 km, maximum = 71 km) can be generated for $e = 0.02$, $a = 20\ R_E$, $T_b = 1175$°C, and $q_o = 27$ mW/m$^2$ (Fig. 2). The mean thickness is slightly higher than the present estimate of ~45 km, but it is lower than present farside values. The value of $a$ corresponds to up to tens of million years of lunar evolution, during which the crust may have grown by tens of kilometers (SOM), relatively consistent with the calculated thickness, given our uncertainty in early orbital evolution. Further, the value of $e$ is not inconsistent with our knowledge of the early lunar eccentricity (SOM). The value of $T_b$ is reasonable based on the temperature of late-stage crystallization products [for instance, KREEP basalt liquidus of ~1185°C (*23*); pyroxene-ilmenite cumulate solidus of ~1125°C (*24*)] (SOM).

The net crustal-thickness difference arising from dissipation depends on numerous orbital and thermal parameters that are difficult to constrain precisely (*25*). Higher differences may result from a basal partially molten zone (*26*) (SOM), a different rheology, higher $e$, or higher $T_b$. For example, the use of the above parameters (with $T_b = 1225$°C and $q_o = 30$ mW/m$^2$) yields a crustal-thickness amplitude of 44 km (mean thickness = 39 km), which is close to the observed values. Such a temperature may be too hot for late-stage magma-ocean liquids

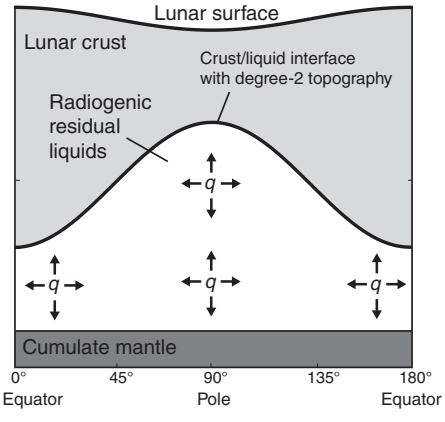


**Fig. 3.** Degree-2 basal topography on the crust also causes degree-2 variations in magma-ocean thickness, such that higher total heat production will be found beneath regions of thinner crust, possibly influencing crustal crystallization. $q$, volumetric heat production. Image not shown to scale.

(SOM), but it illustrates the effect of increased dissipation.

Despite these uncertainties in crustal amplitude, the detailed crustal-thickness pattern is very similar for all models in which dissipation is strong, and it can, therefore, be used to test our predictions (Fig. 2, SOM, fig. S12). The crustal-thickness patterns in swaths 3 to 5 are in good agreement with amplitude-scaled tidal model data (*27*), over the regions plotted on the globe in Fig. 2B, except for the effect of SP-A. Swath 1 has good agreement over ~90° of arc, but is poorer elsewhere. Swath 2 has good agreement from –90° to +50° and also predicts the terrain labeled "X" in Fig. 1. Generally, the lack of agreement is due to the superposition of a weak pole-to-equator surface temperature effect and degree-4 harmonic on the model's stronger degree-2 pattern (SOM). Note that swath 2 shows evidence of the predicted degree-4 harmonic at site X. The case for $T_b = 1225$°C gives even better agreement in shape without any rescaling of the actual crustal thickness (fig. S10).

Though there is disagreement between model and observations in some locations, the model shows clear evidence for a degree-2 pattern that dominates higher-order effects (SOM). Physically, the imperfect agreement may be due to subsequent thermal processes that altered the distribution of crustal thickness near the PKT and elsewhere (*28*). Alternatively, polar wander about the axis through the primordial sub and anti-Earth points (*29*) could have averaged out harmonics other than the dominant degree-2 harmonic. In addition, lower crustal flow may have preferentially removed the higher-order degree-4 thickness variations (SOM). Most importantly, however, whereas other large-scale geophysical processes (such as convection and Rayleigh-Taylor instabilities) can be described mathematically in spherical harmonics, there is no simple reason that they must manifest themselves geologically with a predominantly $P_2$ shape (SOM), in contrast to the tidal-dissipation mechanism discussed here. Therefore, early tidal dissipation is presently the strongest candidate for the formation of the DTT.

A consequence of tidally driven crustal-thickness variations is that the subsurface magma ocean will be thicker and thinner in regions of thinner and thicker crust, respectively, assuming negligible mantle topography (Fig. 3). Because magma-ocean liquids are enriched in radiogenic elements (*4*), regions of thinner crust will have higher subsurface heat production than regions of thicker crust. Depending on the ocean depth and vigor of convective heat redistribution, this variable heat production may further influence crustal crystallization (SOM) (*3*) and global ocean convection patterns.

A tidally driven crust-building mechanism would have likely once had global symmetry. A second region of thickened crust would have been centered antipodal to the DTT at present day (0°N, 35°E), and the present PKT would have been approximately between them (Fig. 2B). In the 4.4 billion years after the magma-ocean epoch, many geologic processes may have altered and diminished the evidence for this crust-building process on the other ~76% of the Moon, such as large impact basins, long wavelength thermal-compositional events (*28*), and volcanism. However, the relict of that epoch identified here has linked two previously disparate sections of the Moon and implicates the role of ancient tidal processes in defining the present-day structure of the lunar crust.

### References and Notes


1. W. M. S. Kaula, G. Schubert, R. E. Lingenfelter, W. L. Sjogren, W. R. Wollenhaupt, *Proc. Lunar Sci. Conf.* **5**, 3049 (1974).
2. B. L. Jolliff, J. J. Gillis, L. A. Haskin, R. L. Korotev, M. A. Wieczorek, *J. Geophys. Res.* **105**, 4197 (2000).
3. J. T. Wasson, P. H. Warren, *Icarus* **44**, 752 (1980).
4. C. K. Shearer *et al.*, *Rev. Mineral. Geochem.* **60**, 365 (2006).
5. M. T. Zuber, D. E. Smith, F. G. Lemoine, G. A. Neumann, *Science* **266**, 1839 (1994).
6. J. A. Wood, *Moon* **8**, 73 (1973).
7. D. E. Loper, C. L. Werner, *J. Geophys. Res.* **107**, 5046 (2002).
8. D. E. Smith *et al.*, *Geophys. Res. Lett.* **37**, L18204 (2010).
9. N. Namiki *et al.*, *Science* **323**, 900 (2009).
10. D. E. Smith, M. T. Zuber, G. A. Neumann, F. G. Lemoine, *J. Geophys. Res.* **102**, 1591 (1997).
11. M. A. Wieczorek, R. J. Phillips, *Icarus* **139**, 246 (1999).
12. I. Garrick-Bethell, M. T. Zuber, *Icarus* **204**, 399 (2009).
13. D. E. Wilhelms, *The Geologic History of the Moon*. *U.S. Geological Survey (USGS) Professional Paper 1348* (USGS, Denver, CO, 1987).
14. S. Zhong, M. T. Zuber, *J. Geophys. Res.* **105**, 4153 (2000).
15. S. C. Solomon, J. Longhi, *Proc. Lunar Sci. Conf.* **8**, 583 (1977).
16. A. Nemchin *et al.*, *Nat. Geosci.* **2**, 133 (2009).
17. H. Jeffreys, *The Earth* (Cambridge Univ. Press, Cambridge, 1976).
18. G. W. Ojakangas, D. Stevenson, *Icarus* **81**, 220 (1989).
19. F. Nimmo, P. C. Thomas, R. T. Pappalardo, W. B. Moore, *Icarus* **191**, 183 (2007).
20. G. Tobie, A. Mocquet, C. Sotin, *Icarus* **177**, 534 (2005).
21. F. Nimmo, B. G. Bills, *Icarus* **208**, 896 (2010).
22. E. Rybacki, G. Dresen, *J. Geophys. Res.* **105**, 26017 (2000).
23. P. C. Hess, M. J. Rutherford, H. W. Campbell, *Proc. Lunar Sci. Conf.* **9**, 705 (1978).
24. J. A. Van Orman, T. L. Grove, *Meteorit. Planet. Sci.* **35**, 783 (2000).
25. Crustal-thickness differences may also be lowered as the remaining liquids under the crust crystallize (SOM section 8).
26. E. M. Parmentier, Y. Liang, in *41st Lunar and Planetary Science Conference (LPSC)*, *Abstract 1824* (LPSC, The Woodlands, TX, 1 to 5 March 2010).
27. We have multiplied the actual crustal thickness by 0.4 to better match the thickness amplitudes in the two cases.
28. E. M. Parmentier, S. Zhong, M. T. Zuber, *Earth Planet. Sci. Lett.* **201**, 473 (2002).
29. G. W. Ojakangas, D. J. Stevenson, *Icarus* **81**, 242 (1989).


30. We thank E. M. Parmentier, G. Hirth, L. Elkins-Tanton, M. T. Zuber, J. Andrews-Hanna, G. A. Glatzmaier, P. C. Hess, and M. J. Rutherford for helpful discussions. This work was made possible by a Brown University postdoctoral research assistantship to I.G.-B.


### Supporting Online Material

www.sciencemag.org/cgi/content/full/330/6006/949/DC1
SOM Text
Figs. S1 to S17
Tables S1 to S5
References

8 June 2010; accepted 7 October 2010
10.1126/science.1193424